Journal of the Mechanical Behavior of Biomedical Materials 172 (2025) 107183

Contents lists available at ScienceDirect

Journal of the Mechanical Behavior of Biomedical Materials

journal homepage: www.elsevier.com/locate/jmbbm

Therapeutic potential of COMP and TIMP-3 in preserving cartilage integrity compromised by proteases: A histo-mechanical study

Asif Istiak [a], Austin Lawrence [b], Joseph Boesel [b], Md Imrul Kayes [a], Ahmed Suparno Bahar Moni [b], Tanvir R. Faisal [a,*]

[a] Department of Mechanical Engineering, University of Louisiana at Lafayette, LA, 70503, USA
[b] Department of Orthopedics and Medical Education, College of Medicine and Life Sciences, University of Toledo, OH, 43614, USA

ARTICLE INFO

Keywords:
Articular cartilage
MMP
ADAMTS
COMP
Biomechanics
TIMP

ABSTRACT

Matrix metalloproteinases (MMPs) and a disintegrin and metalloproteinase with thrombospondin motifs (ADAMTS) significantly impact articular cartilage biomechanical properties in osteoarthritis (OA). However, comprehensive understanding of biomechanical responses and the efficacy of potential therapeutic interventions remains limited. This study investigates how MMPs and ADAMTS synergistically degenerate cartilage biomechanical properties under different loading conditions, and evaluates the preventive role of cartilage oligomeric matrix protein (COMP) and tissue inhibitor of metalloproteinase-3 (TIMP-3). Bovine tibiofemoral cartilage disks (N = 80) with subchondral bone from 8 cows were harvested and incubated with MMP-9, MMP-13, ADAMTS-5, COMP, and TIMP-3 in four distinct combinations: Group A (MMP-9+MMP-13+ADAMTS-5), Group B (Group A + COMP), Group C (Group A + TIMP-3), Group D (Group B + TIMP-3) and Group E (negative control). Comprehensive biomechanical assessment included indentation, unconfined compression, and dynamic testing to simulate various physiological activities. Safranin O and Picrosirius red staining were used for histological analysis. Group A demonstrates reduced Young's modulus 71.7% (95% confidence interval (CI) : [64.3%, 85.2%]), instantaneous modulus 71.4% (95% CI : [50.0%, 83.6%]), and equilibrium modulus 61.7% (95% CI : [24.6%, 80.6%]) compared to controls. Adding COMP substantially improved Young's modulus 41.4% (95% CI : [9.9%, 102.2%]) and equilibrium modulus 18.9% (95% CI : [−31.9%, 107.8%]) relative to Group A. Supplementation with TIMP-3 exhibited significant improvements in strain-dependent instantaneous modulus and dynamic modulus by 235.5% (95% CI : [117.7%, 417.9%]) and 178.6% (95% CI : [100.4%, 296.3%]) respectively. Histological assessment confirmed improvement in proteoglycan and collagen preservation across treatment groups. This study suggests that COMP helps preserve cartilage mechanical integrity by indirectly protecting cartilage from all the applied proteases, while TIMP-3 provides substantial additional protection through direct inhibition of MMP-13 and ADAMTS-5. The investigations suggest activity-specific recommendations for OA management and provide valuable insights into developing targeted OA interventions.

1. Introduction

The mechanical performance of articular cartilage is fundamentally dependent on its complex extracellular matrix (ECM) constituents and organization, and its response to various physiological activities. In healthy cartilage, the mechanical response and tissue homeostasis rely primarily on the structural integrity of collagen fibrils and the abundance of aggrecan content. Type II collagen fibril, through its unique triple-helical structure and extensive cross-linking, provides tensile strength, compressive stiffness, and resistance to deformation (Hu et al., 2024). Proteoglycans (PGs), particularly aggrecan—the large aggregating proteoglycan, contribute to the tissue's viscoelastic behavior and elastic stiffness during impact loading by regulating fluid distribution through swelling/osmotic pressure, while also facilitating controlled deformation under sustained load (Kiani et al., 2002). This intricate balance between structural components enables cartilage to maintain its

* Corresponding author. Department of Mechanical Engineering, University of Louisiana at Lafayette, 241 E Lewis St., Lafayette, LA, 70503, USA.
E-mail addresses: asif.istiak1@louisiana.edu (A. Istiak), austin.lawrence@rockets.utoledo.edu (A. Lawrence), joseph.boesel@rockets.utoledo.edu (J. Boesel), md-imrul.kayes1@louisiana.edu (M.I. Kayes), AhmedSuparno.BaharMoni@UToledo.Edu (A.S. Bahar Moni), tanvir.faisal@louisiana.edu, tanvir.faisal@mail.mcgill.ca (T.R. Faisal).

https://doi.org/10.1016/j.jmbbm.2025.107183
Received 2 June 2025; Received in revised form 16 August 2025; Accepted 31 August 2025
Available online 2 September 2025
1751-6161/© 2025 Published by Elsevier Ltd.

crucial role in joint function and mobility.

While regulated levels of matrix metalloproteinases (MMPs) and a disintegrin and metalloproteinase with thrombospondin motifs (ADAMTS) are necessary for normal ECM maintenance and remodeling, their dysregulation in conditions like osteoarthritis (OA) initiates a cascade of destructive events. This disruption compromises tissue structure and mechanical integrity through irreversible collagen cleavage and PG degradation (Takahashi et al., 2005). Classically, MMPs play a dominant role in the breakdown of ECM macromolecules and are collectively capable of degrading all the ECM components (Grenier et al., 2014). PG depletion is thought to be an earlier and reversible process initiated by the MMPs and ADAMTSs in articular cartilage (Galloway et al., 1983; Karsdal et al., 2008), whereas the breakdown of the collagen network is believed to be the point of no return once the disease progresses further.

MMPs that have been largely implicated in the pathogenesis of OA are grouped into collagenases (MMPs-1, 8, and 13), and gelatinases (MMPs-2 and 9) and are all expressed at low levels in healthy joints (Davidson et al., 2006; Meszaros and Malemud, 2012; Sandy, 2006; Struglics et al., 2006). These enzymes act in two steps; first collagenases (MMPs-1, 8 or 13) cleave and bind triple helical collagen molecules and denature the collagen fibrils (Powell et al., 2019; Rosenblum et al., 2010; Sarkar et al., 2012). Afterwards, gelatinases (MMPs-2, 9) digest the denatured fibrils (Atkinson et al., 2001; Collier et al., 2011; Rosenblum et al., 2010). However, MMP-13 (collagenase 3) is the major catabolic effector in OA and has been assumed to be more active than MMP-1 on type II collagen (Knäuper et al., 1996; Rose and Kooyman, 2016; Shiomi et al., 2010). The unique destructive potential of MMP-13 lies in its ability to cleave native triple-helical type II collagen at specific sites, leading to rapid deterioration of the collagen network that is essential for cartilage's mechanical stability (Acharya et al., 2014a). In addition, MMP-9 exhibits broad substrate specificity, initially targeting the non-collagenous components of the ECM. It degrades not only aggrecans but also various collagen types (IV, V, VII, and X) and elastin, compromising the tissue's structural integrity at multiple levels (Kim and Hwang, 2011; Mukherjee and Das, 2024; Smith Jr, 2006). Among the MMPs that digest ECM proteins and collagens, MMP-9 and MMP-13 are particularly selected in this study as they are associated with severe OA inflammation, operating through distinct but complementary pathways (Acharya et al., 2014a). Aggrecanases (ADAMTSs-1, 4, 5, 8, 9, and 15) have also demonstrated roles in OA pathology (Santamaria, 2020; Lohmander et al., 1993). Although it has been shown that MMPs could cleave aggrecan (Fosang et al., 1991, 1992, 1993; Sandy et al., 1992; Lohmander et al., 1993), the cleavage activity is primarily attributed to ADAMTS-4 (aggrecanase-1) and ADAMTS-5 (aggrecanase-2) (Abbaszade et al., 1999; Tortorella et al., 2000, 2001; Tortorella and Malfait, 2008). ADAMTS-4 and ADAMTS-5 are thought to analogously mediate aggrecan cleavage; however, prior research evidently shows that ADAMTS-5 serves as a primary mediator of aggrecan degradation through its proteolytic activity across multiple aggrecan domains (Apte, 2016; Glasson et al., 2004, 2005; Jiang et al., 2021). The rationale for using ADAMTS-5 is its destructive behavior when working combinedly with MMPs, as the combined degradation of both collagen and PGs severely compromises tissue's mechanical properties. Therefore, the current study considered MMPs-13, 9 and ADAMTS-5 synergistically to emulate severe osteoarthritic conditions *in vitro*.

The cartilage oligomeric matrix protein (COMP) has emerged as an established OA biomarker, exhibits elevated levels in response to inflammatory cytokines, mechanical loading, and ECM degeneration (Cui and Zhang, 2022; Kersting et al., 2005). However, its role in OA pathogenesis presents an intriguing paradox: while COMP is expressed during ECM degeneration, it contributes to defect delocalization, collagen secretion, binding with protease and ECM stability, it can simultaneously increases tissue invasiveness by triggering gelatinase activity (Acharya et al., 2014a; Englund et al., 2016; Posey et al., 2018; Tseng et al., 2009). This dual nature suggests potential therapeutic opportunities if its beneficial effects can be harnessed while minimizing its destructive potential.

The tissue inhibitor of metalloproteinases (TIMP), particularly TIMP-3 represents a promising therapeutic approach due to its ability to limit cartilage degradation through strong affinity for various MMPs and ADAMTS family members (Brew and Nagase, 2010; Carreca et al., 2020). Understanding the precise mechanisms of TIMP-3 interaction with these proteases is crucial for developing more effective therapeutic strategies. The internal load-bearing components of cartilage demonstrate distinct responses under varying physiological conditions, and these mechanical characteristics fluctuate with morphological changes across different OA stages (Ebrahimi et al., 2019; Kabir et al., 2021; Korhonen et al., 2002; Linus et al., 2024). Despite this understanding, comprehensive analyses of *in vivo* and *in vitro* morpho-biomechanical alterations in enzyme-mediated osteoarthritic cartilage remain limited and lack comprehensive analysis (Istiak et al., 2025; Marouane et al., 2016).

In this study, we developed an advanced osteoarthritic condition *in vitro* using MMP-13 (collagenase), MMP-9 (gelatinase), and ADAMTS-5 (aggrecanase). With this model, we developed a comprehensive approach to understanding the complex interplay between enzymatic degradation and mechanical loading in OA progression. A novel therapeutic intervention using COMP with TIMP-3 was further investigated to address critical gaps in potential treatments, inhibiting enzymatic degeneration. These findings have immediate clinical relevance, potentially contributing to the development of more effective treatment for OA patients and advancing our understanding of how mechanical loading regimens might be optimized for different stages of the disease. Ultimately, by elucidating the relationships between enzymatic activity, mechanical properties, and therapeutic interventions, this study lays groundwork for developing more targeted and effective treatments for OA.

2. Materials and methods

2.1. Sample preparation

Fresh stifle joints of 8 healthy cows between 18 and 36 months of age were collected from the local abattoir. Cylindrical osteochondral explants (N = 80, d = 9 mm) were extracted in equal number from femoral condyle and tibial condyle of the stifle joints using surgical power drill. 60 (5 groups; n = 12/group) and 20 (5 groups; n = 4/group) specimens were selected randomly without any bias corresponding to the donor animal and sites, and randomized block (equal) corresponding to two condyles for the purposes of conducting biomechanical assessments and histological analyses, respectively (Festing, 2020). Cartilage showing any visible fissures or surface defects were excluded from the current study. Using ImageJ (National Institute of Health), cartilage thickness was measured from the high-resolution image of the cartilage disks. The average thickness of articular cartilages was 1.86 ± 0.35 *mm* of 3.5 ± 0.5 *mm* osteochondral disks. The samples were stored frozen at $-20^{\circ}C$ in phosphate-buffered saline (PBS) moistened gauze prior to testing. The samples were thawed at room temperature for 45 min in the PBS filled vials prior to incubation and biomechanical testing.

2.2. Enzymatic degradation

The cartilage plugs were transferred to sterile agar plates and gently embedded in a solidified 2 % agarose gel to secure the plugs during enzyme treatment. The agarose gel was prepared by dissolving 50 g of agarose in 2500 mL of 1x TAE buffer, autoclaving, and then solidifying the agarose in culture plates. The samples were incubated in a combination of activated MMP-9 and MMP-13, ADAMTS-5, COMP, and TIMP-3 in five different study cohorts (n = 12) in PBS medium at $37^{\circ}C$ for 44 h, with gentle agitation in every 10–12 h. Each group of cartilage plugs was exposed to a specific combination of these enzymes (Table 1) to simulate

Table 1
Concentration of MMPs-9 and 13, ADAMTS-5, COMP and TIMP-3, considered in this work, to treat articular cartilage samples.

Group Enzyme concentration	Group A (M + A)	Group B (M + A + C)	Group C (M + A + T)	Group D (M + A + C + T)	Group E (Negative control)
MMP-9 (ng/mL) (Jarecki et al., 2022; Stojanovic et al., 2023)	30	30	30	30	
MMP-13 (ng/mL) (Heard et al., 2012; Wang et al., 2004)	15	15	15	15	
ADAMTS-5 (ng/mL) (Hao and Wu, 2024; Zhang et al., 2013)	15	15	15	15	
COMP (ng/mL) (Plsikova Matejova et al., 2021)		5000		5000	
TIMP-3 (ng/mL) (Carreca et al., 2020)			200	200	

severe erosive OA as well as subsequent treatment (Carreca et al., 2020; Hao and Wu, 2024; Meehan et al., 2021; Plsikova Matejova et al., 2021; Stojanovic et al., 2023). The concentration of MMP-13 (Heard et al., 2012; Wang et al., 2004) and ADAMTS-5 (Hao and Wu, 2024; Zhang et al., 2013) was selected from both *in vivo* and *in vitro* immunoassays (ELISA) test from advanced osteoarthritic condition. The selection of concentration of MMP-9 (Jarecki et al., 2022; Stojanovic et al., 2023) and COMP (Plsikova Matejova et al., 2021) was selected from *in vivo* investigation of advanced and erosive osteoarthritis. High amount of COMP is secreted to compromise the damage (Cui and Zhang, 2022; Koelling et al., 2006), this concentration was selected for therapeutic intervention. According to the prediction of enzyme kinetic theory (Bieth, 1995) and *in vitro* test (Carreca et al., 2020), equimolar TIMP-3 compared to degenerative enzymes shows incomplete inhibition. However, MMP-13 (Carreca et al., 2020) and ADAMTS-5 (Carreca et al., 2020; Troeberg et al., 2009) can be completely inhibited respectively 1 nM and around 10 nM, and MMP-9 cannot disrupt the inhibition ability of TIMP-3 (Carreca et al., 2020). Considering calculated molecular weight, 21.6 kDa of TIMP-3 (Wetzel et al., 2008), the concentration dose for this study was determined as 200 ng/mL. All enzymes were purchased from Sigma Aldrich. Table 1 shows the concentration of the enzymes per study cohort.

Enzymatically treated cartilage explants were washed and transferred to a serum-free medium (low glucose Dulbecco's Modified Eagles Medium [DMEM; 1 g/l]) supplemented with 10 mM HEPES buffer, 0.1 mM nonessential amino acids, 0.4 mM proline, 20 μg/ml ascorbate, 100 U/ml PenStrep, and 10 % fetal bovine serum (FBS) to incubate at 37 °C using 5 % CO_2 and equilibrated for 2 days prior to experiments to prevent further degradation of cartilage in the intervals of mechanical tests.

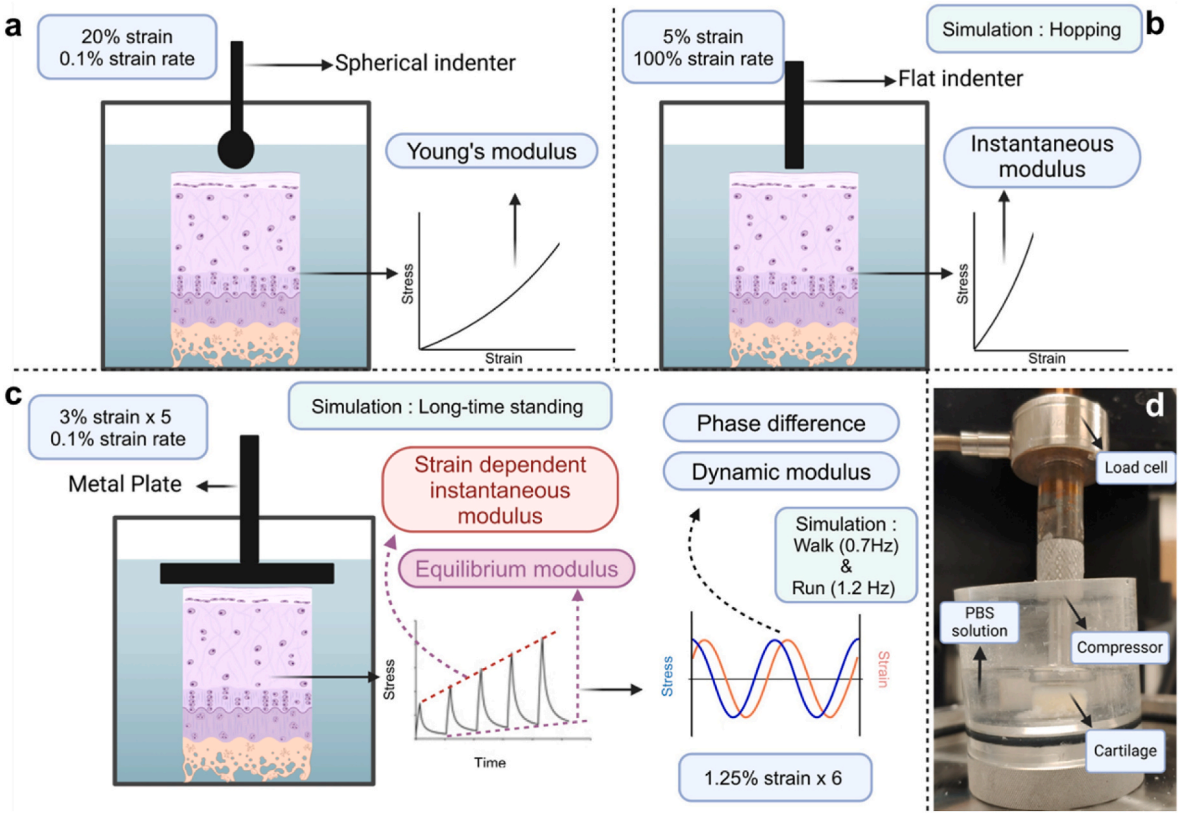

Fig. 1. Systematic biomechanical testing methodology for osteochondral samples. (a) Spherical indentation test configuration to determine Young's modulus, where the indenter applies a 20 % strain at 0.1 % strain rate (Istiak et al., 2025). (b) Fast indentation utilizing a flat indenter to measure instantaneous modulus, simulating high-impact activities such as hopping or jumping through a 5 % strain application at 100 % strain rate (Kabir et al., 2021). (c) Stress-relaxation test incorporating a five-step compression sequence at 3 % strain per step to evaluate both strain dependent instantaneous modulus (at 0.1 % strain rate) and equilibrium modulus. This testing sequence is followed by sinusoidal loading to determine dynamic modulus and phase difference for walking and running (Niehoff et al., 2011; Strutzenberger et al., 2021). (d) Complete experimental setup in the Mach-1 testing system, showing the cartilage disk specimen submerged in the PBS solution positioned under the mechanical compressor.

2.3. Biomechanical testing

Mechanical tests were conducted blindly using a Mach-1 v500c (Biomomentum Inc.) micromechanical tester with a testing protocol designed to simulate various physiological loading conditions sequentially on the same sample. To ensure reliable data collection, each sample underwent a standardized series of tests with a minimum two-hour relaxation period between consecutive assessments (Korhonen et al., 2002; Mixon et al., 2021, 2022). Each sample was attached with its subchondral region to a custom sample holder filled with PBS using an acrylate-based adhesive. Fig. 1 presents a detailed schematic illustration of different biomechanical testing configurations.

To evaluate the Young's modulus (E) of articular cartilage under normal physiological conditions, we performed a slow single-step indentation test using a spherical indenter with a diameter of 2 mm. The test protocol implemented a strain rate of 0.1 % and applied a total strain of 20 % of the cartilage thickness. The Young's modulus was determined using the Mach-1 analyzing software, which incorporates the Hertz and Hayes model (Hayes et al., 1972) as follows:

$$E = \frac{2P(1-\nu^2)}{4\kappa\omega_0^{3/2}\sqrt{R\chi}} \tag{1}$$

$$E = \frac{P(1-\nu^2)\pi a}{2\kappa h} \tag{2}$$

where P is the stress-strain ratio collected from the Mach-1 analyzing software, ν is the Poisson's ratio ($\nu = 0.3$ for equilibrium and steady condition; $\nu = 0.5$ for instantaneous and incompressible condition) (Linus et al., 2024). κ and χ are the variable dependent on the cartilage thickness and indenter diameter which were iterated from Hayes table (Hayes et al., 1972). ω_0 is the indenter displacement recorded by the Mach-1 software and R is the radius of the indenter, a is the indenter diameter and h is the cartilage thickness.

To assess high impact loading, a flat indenter with a diameter of 2 mm was selected specifically to achieve uniform stress distribution during instantaneous (rapid) compression. A high strain rate loading protocol was considered (Fig. 1b) to account for increased pore pressurization during rapid compression (Nguyen and Levenston, 2012). The instantaneous modulus calculations incorporated geometric corrections based on Hayes model (Eq. (2)), accounting for both indenter dimensions and cartilage thickness in the analysis. A prestress of 12.5 kPa was applied to ensure consistent and reliable measurements, confirming optimal contact between the platen and cartilage surface (Korhonen et al., 2002).

We performed unconfined stress relaxation testing using a 12 mm diameter non-porous platen. The loading protocol began with an initial 5 % strain (prestressed). A total of 15 % strain relative to cartilage thickness was applied equally in 5 steps at a strain rate of 0.1 % with a relaxation period of 180 s following each compression that allowed the tissue to achieve equilibrium. The strain dependent (slow rate) instantaneous modulus, E_{inst}, was calculated using equation (3).

$$E_{inst} = E^{o}_{inst} + E^{\varepsilon}_{inst}\varepsilon \tag{3}$$

where E^{o}_{inst} is the initial instantaneous modulus, E^{ε}_{inst} is measured from the slope of a linear fit applied to the instantaneous stress values recorded during each phase of the stress-relaxation process, and ε is the strain, . The equilibrium modulus was calculated from the slope of the line connecting the equilibrium points from the second through final loading steps.

We implemented a sinusoidal loading protocol following the stress-relaxation assessments—representative of daily activities. Following stress-relaxation, a cyclic load of 1.25 % strain was applied over six cycles (Fig. 1c) at a frequency of 0.7 Hz and 1.2 Hz to simulate walking and running activities, respectively. The dynamic modulus was determined by calculating the ratio between peak stress and corresponding peak strain values during cyclic loading. Additionally, the phase difference was measured by analyzing the temporal offset between peak stress and peak strain responses, providing insight into the tissue's viscoelastic behavior under dynamic loading conditions.

2.4. Histological analysis

To facilitate histological analysis, articular cartilage was separated from the subchondral bone to avoid decalcification process. After dehydrating in a series of graded (50 %–100 %) alcohol, the samples were fixed in Paraplast Plus paraffin. Afterwards, 5 μm thick slices were sectioned with a microtome (Shandon Scientific; model: Finesse ME). After deparaffinizing, the cartilage slices were stained with Safranin O (Sigma-Aldrich), without counter stain Fast Green (Alibegović et al., 2020), to evaluate PGs using light microscope and Picrosirius red (Sigma-Aldrich) for detecting collagen content by polarized light microscope (PLM). The micrographs were qualitatively graded by 10 blind experts independently (Alibegović et al., 2020; Kositsky et al., 2025) following modified histological score (Glasson et al., 2010; Mixon et al., 2021).

2.5. Statistical analysis

Statistical analyses were performed using a combination of custom-developed Python code and OriginPro, Version 2024b (OriginLab Corporation, Northampton, MA). All the independent variables—modulus (mechanical test results) were normally distributed (Shapiro-Wilk test: $p > 0.05$) (Kositsky et al., 2025) except instantaneous and equilibrium modulus. Levene's test ($p > 0.05$) was conducted to further assess the homogeneity of variance (homoscedasticity) of the normally distributed variables (Veronesi et al., 2015). After that, Welch's ANOVA (Maenohara et al., 2020) and Games Howell post hoc tests were conducted to assess significant difference among groups. For non-parametric variable, Kruskal-Wallis test followed by Dunn's post hoc test was used to evaluate inter group statistical difference (Mixon et al., 2021). To measure inter group difference, Gamma Generalized Linear Model (GLM) was used to check the residuals of the dataset. Gamma GLMs compare arithmetic means multiplicatively via log-link coefficients and provides ratio using confidence interval (CI). To ensure the reliability of our observational data, we calculated the Fleiss-type weighted kappa coefficient to assess interobserver variability in our (histology) measurements. Furthermore, the Pearson correlation test was used to assess the relationship between mechanical responses and histological assessments.

3. Results

3.1. Biomechanical properties

The biomechanical properties assessed through a series of mechanical testing revealed distinct patterns across experimental groups, as primarily illustrated in Figs. 2–4.

3.1.1. Young's modulus

The negative control (Group E) exhibits a mean Young's modulus of 0.87 ± 0.27 *MPa* (Fig. 2a) and is consistent with our prior work (Istiak et al., 2025; Mixon et al., 2021, 2022). The Young's modulus of Group A (M + A) is (0.20 ± 0.06 *MPa*), Group B (M + A + C) is (0.28 ± 0.18 *MPa*), Group C (M + A + T) is (0.35 ± 0.13 *MPa*) and Group D (M + A + C + T) is (0.41 ± 0.27 *MPa*) as shown in Fig. 2a. The healthy cartilage (Group E) demonstrates markedly higher mechanical properties, with significant mean differences of 71.7% ($p < 0.001$, 95% CI by GLM : [64.3%, 85.2%]), 67.6% ($p < 0.001$, 95% CI : [50.2%, 78.9%]), 59.7% ($p < 0.001$, 95% CI : [23.1%, 89.5%]) and 52.2% ($p < 0.001$, 95% CI : [26.6%, 68.9%]) when compared with Groups A, B, C and D respectively.

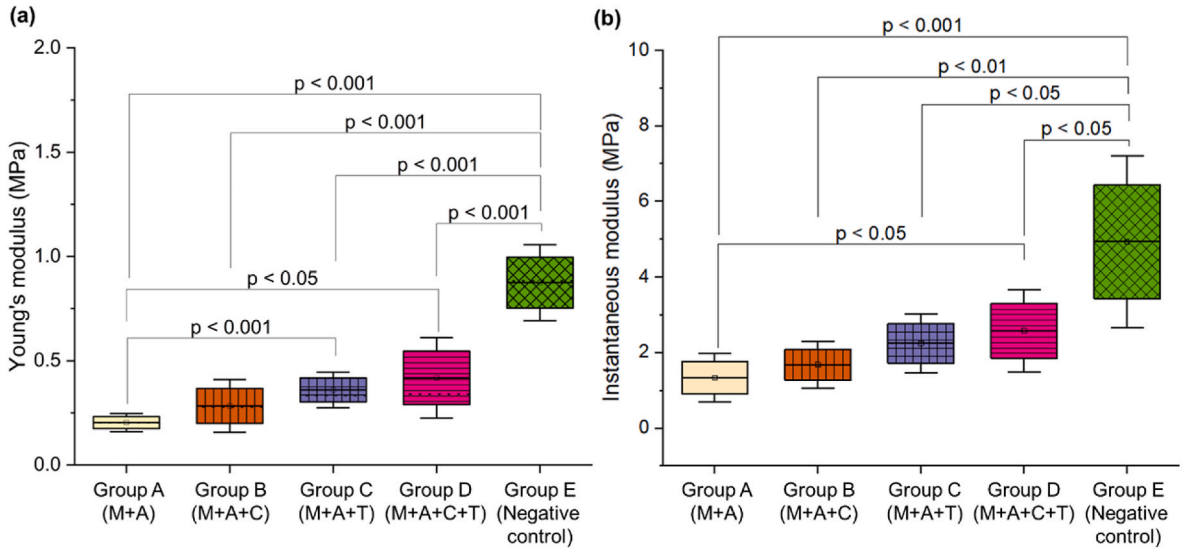

Fig. 2. Box whisker plots show distribution of (a) Young's modulus (E) and (b) instantaneous modulus (E_{inst}) with individual data points of each treatment group (n = 12 per group). The error bar represents 95 % CI. Mean and median of the distributions in all figures are represented by solid and dotted horizontal line, respectively. For all statistical comparisons, the statistical significances are shown as $p < 0.001$, $p < 0.01$, and $p < 0.05$ unless *p-values* are non-significant. Group A (M + A): samples treated with MMP-9, MMP-13 and ADAMTS-5, Group B (M + A + C): samples treated with MMP-9, MMP-13, ADAMTS-5 and COMP, Group C (M + A + T): samples treated with MMP-9, MMP-13, ADAMTS-5 and TIMP-3, Group D (M + A + C + T): samples treated with MMP-9, MMP-13, ADAMTS-5, COMP and TIMP-3, and Group E (Negative control) denotes healthy samples.

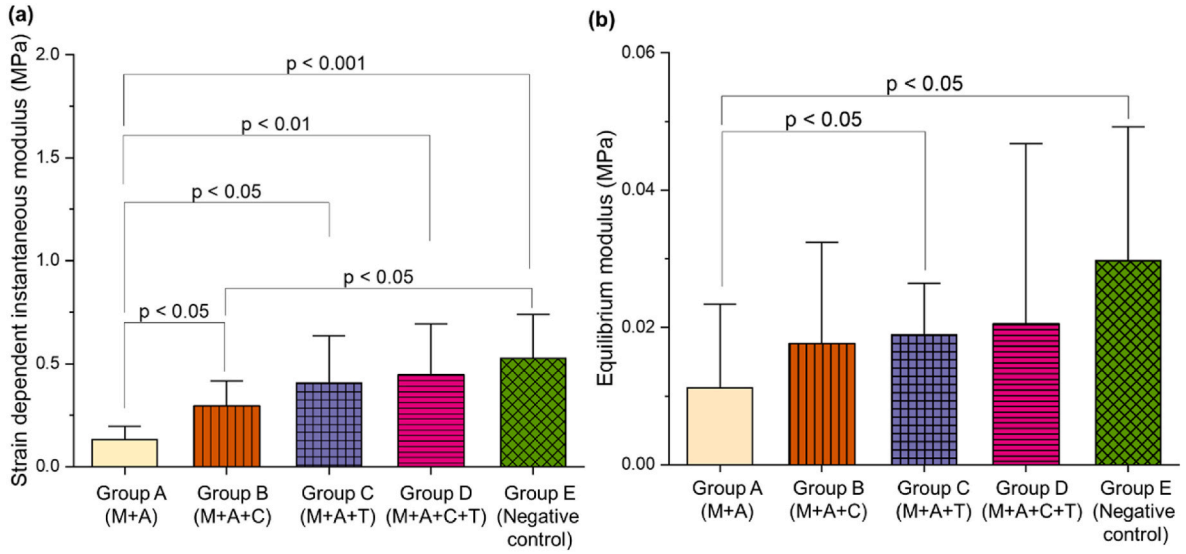

Fig. 3. Stress-relaxation properties of articular cartilage. Bar plots showing the distribution of strain-dependent instantaneous modulus (a) and equilibrium modulus (b) for each experimental group (n = 12 per group). The error bar represents 95 % CI. For all statistical comparisons, the statistical significances are shown as $p < 0.001$, $p < 0.01$, and $p < 0.05$ unless *p-values* are non-significant. Group A (M + A): samples treated with MMP-9, MMP-13 and ADAMTS-5, Group B (M + A + C): samples treated with MMP-9, MMP-13, ADAMTS-5 and COMP, Group C (M + A + T): samples treated with MMP-9, MMP-13, ADAMTS-5 and TIMP-3, Group D (M + A + C + T): samples treated with MMP-9, MMP-13, ADAMTS-5, COMP and TIMP-3, Group E (Negative control) denotes healthy samples.

3.1.2. Instantaneous modulus

In Fig. 2b, the mean instantaneous modulus of Group A (M + A), Group B (M + A + C), Group C (M + A + T) and Group D (M + A + C + T) are 1.33 ± 0.89 *MPa*, 1.67 ± 0.87 *MPa*, 2.24 ± 1.21 *MPa*, and 2.47 ± 1.63 *MPa*, respectively, with no statistically significant differences among them but Group A shows statistically significant difference with Group D and the negative control in Group E with a mean E_{inst} of 4.93 ± 3.18 *MPa*.

3.1.3. Strain dependent instantaneous modulus

Stress-relaxation properties exhibit distinctive patterns across all the 5 groups (Fig. 3a). The mean (slow) strain dependent instantaneous modulus of negative control (0.52 ± 0.34 *MPa*) shows statistically significant difference with Group A (0.13 ± 0.1 *MPa*) and Group B (0.29 ± 0.19 *MPa*) except Group C (0.40 ± 0.32 *MPa*) and Group D (0.44 ± 0.36 *MPa*). However, Group C and D show statistically significant difference with Group A (M + A).

3.1.4. Equilibrium modulus

Group A, indicating the minimal mechanical performance with the lowest mean equilibrium modulus 0.01 ± 0.01 *MPa*, exhibits a statistically significant difference with negative control (Fig. 3b). The

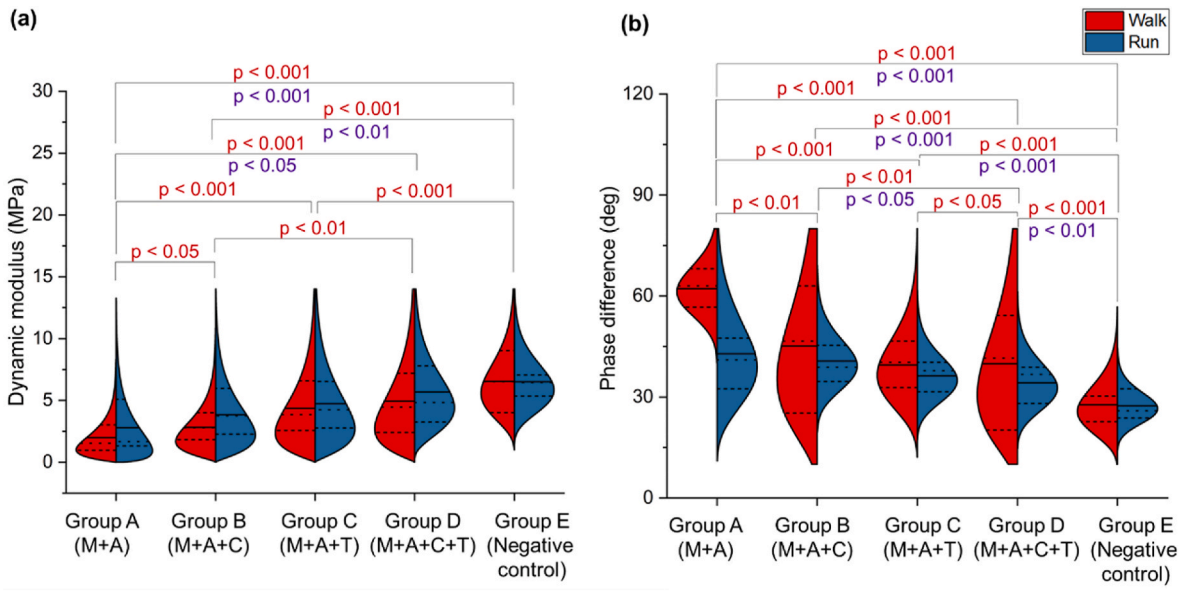

Fig. 4. Dynamic properties of each treatment group (n = 12 per group) of articular cartilage. Half-violin plots demonstrate the dynamic modulus (a) and phase-difference (b) distributions under walking (red) and running (blue) activities. Dash-dot lines represent the lower and the upper level of 95 % CI in half violin plot. Mean and median of the distributions in all figures are represented by solid and dotted horizontal lines, respectively. For all statistical comparisons, the statistical significances are shown as $p < 0.001$, $p < 0.01$, and $p < 0.05$ unless *p-values* are non-significant. *p-values* of walking and running are depicted in red and blue color respectively. Group A (M + A): samples treated with MMP-9, MMP-13 and ADAMTS-5, Group B (M + A + C): samples treated with MMP-9, MMP-13, ADAMTS-5 and COMP, Group C (M + A + T): samples treated with MMP-9, MMP-13, ADAMTS-5 and TIMP-3, Group D (M + A + C + T): samples treated with MMP-9, MMP-13, ADAMTS-5, COMP and TIMP-3, Group E (Negative control) denotes healthy samples.

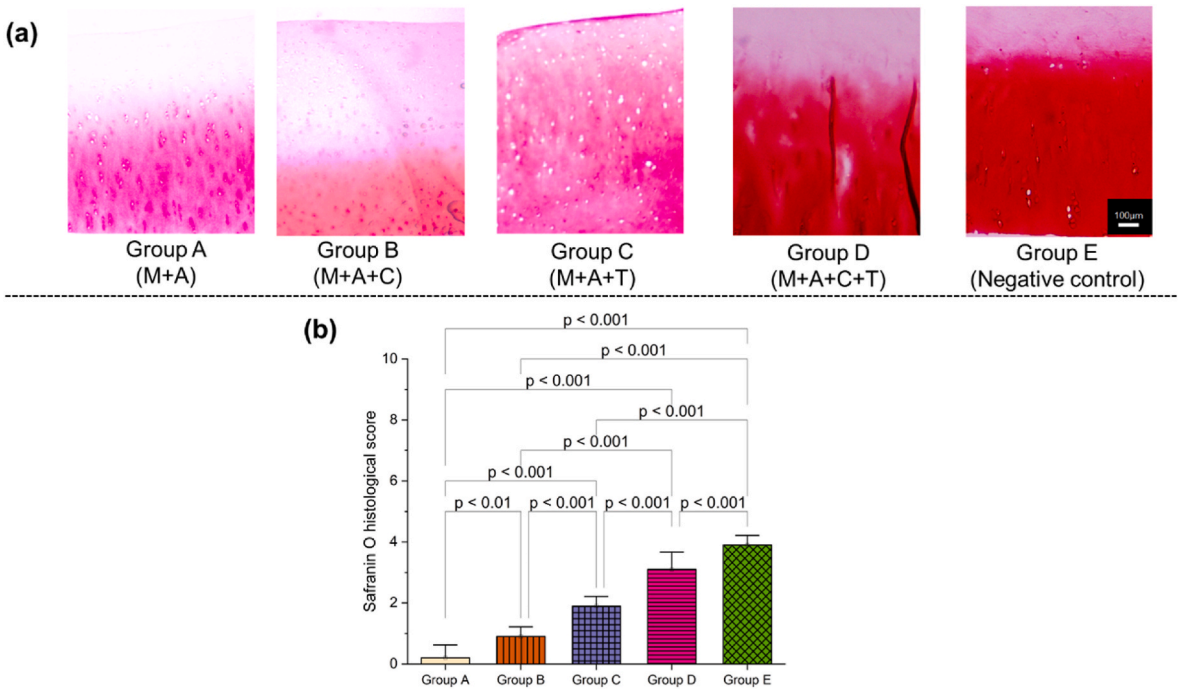

Fig. 5. Histological assessment of each treated group (n = 4 per group) of cartilage tissue, with analysis proceeding according to SZ, MZ and DZ. Note: while partially folded sections shows intensive staining, these regions were excluded from the assessment to maintain analytical accuracy (Alibegović et al., 2020) (a) Representative Safranin O-stained micrographs via light microscopy, demonstrating differential staining patterns across the groups for PG visualization. Scale bar = 100 μm. (b) Semi-quantitative scoring of PG degradation/content classified as minimal (0), very weak (1), weak (2), moderate (3) and strong (4) based on the intensity of the red color. The error bar represents the standard deviation of the grading. The statistical significances are shown as $p < 0.001$, $p < 0.01$, and $p < 0.05$ unless *p-values* are non-significant. Group A (M + A): samples treated with MMP-9, MMP-13 and ADAMTS-5, Group B (M + A + C): samples treated with MMP-9, MMP-13, ADAMTS-5 and COMP, Group C (M + A + T): samples treated with MMP-9, MMP-13, ADAMTS-5 and TIMP-3, Group D (M + A + C + T): samples treated with MMP-9, MMP-13, ADAMTS-5, COMP and TIMP-3, Group E (Negative control) denotes healthy samples.

equilibrium modulus of Group B (M + A + C), Group C (M + A + T), Group D (M + A + C + T) and Group E (negative control) are 0.018± 0.01 *MPa*, 0.019 ± 0.01 *MPa*, 0.021 ± 0.02 *MPa*, and 0.029± 0.02 *MPa*, respectively, excluding the outliers from each (Fig. 3b).

3.1.5. Dynamic modulus and phase difference

The half violin plots in Fig. 4a show the distributions of dynamic modulus for Groups A (M + A), B (M + A + C), C (M + A + T), D (M + A + C + T), and E (negative control) under simulated walking and running conditions. The mean values of the dynamic modulus for the Groups A, B, C, D and E are 1.99 ± 1.35*MPa*, 2.82 ± 1.5*MPa*, 4.35± 2.5*MPa*, 6.46± 3.25*MPa*, and 6.52 ± 2.55*MPa* respectively for walking and 3.17± 2.32*MPa*, 3.83 ± 2.07*MPa*, 4.73 ± 2.9*MPa*, 5.7 ± 2.94*MPa*, and 6.5± 2.2*MPa*, respectively for running. Under walking conditions, statistically significant differences were observed between most group comparisons, except Group B and Group C. While the loading parameters were the same, negative control (Group E) exhibited similar dynamic modulus during walking and running conditions. However, treated groups demonstrated reduced dynamic modulus during walking conditions compared to running.

Phase difference analysis, depicted in Fig. 4b, shows higher values for walking compared with running for all groups, with Group A exhibiting the largest mean value of 62.2 ± 7.5 deg, and 42.8± 14.7 deg for walking and running, respectively. Group E, the healthy cartilage, exhibiting the similar and minimal mean phase differences 27.7 ± 8.04 deg and 27.4 ± 5.0 deg accordingly for walking and running. Notably, while negative control (Group E) maintained consistent phase differences across both walking and running conditions, the treated groups (Groups A, B, C and D) showed higher phase differences during walking compared to running activities.

3.2. Histological analyses

Figs. 5 and 6 show the representative histological image and scores for each group. Figs. 5a and 6a represent the micrographs of Safranin O-stained and Picrosirius red-stained cartilages of each group obtained via light microscopy and PLM, respectively.

3.2.1. Assessment of PG distribution

The Safranin O-stained micrographs demonstrate distinctive patterns of PG distribution across all the Groups A, B, C, D and E, as shown in Fig. 5a. All groups exhibited higher staining intensity in deep zones (DZ) compared to middle zone (MZ) and superficial zone (SZ). However, Groups A and B demonstrated notably lower staining intensity compared to Group D and negative controls, suggesting reduced PG content. Group C shows improved intensity throughout all zones compared with Group A and B. Modified histological scoring (Fig. 5b) shows statistically significant differences across all group comparisons. Groups D and E consistently received high scores with minimal variability, confirming their elevated staining intensity.

3.2.2. Assessment of type II collagen content

Polarized light micrographs of Picrosirius red-stained samples depict the collagen content (Fig. 6a). We observed distinct patterns of collagen content—high-density large collagen fibrils appeared yellow in the SZ, while thin collagen fibrils showed green coloration in the DZ. Group E exhibited the most abundant collagen content, with extensive yellow staining in the SZ and green staining in the DZ as well (Coelho et al., 2018; Cristoforetti et al., 2023; Schmitz et al., 2010). Groups B and C showed reduced and discontinuous collagen content and distribution across all zones compared to group D, while Group A demonstrated minimal collagen presence in the SZ and reduced density in both MZ and

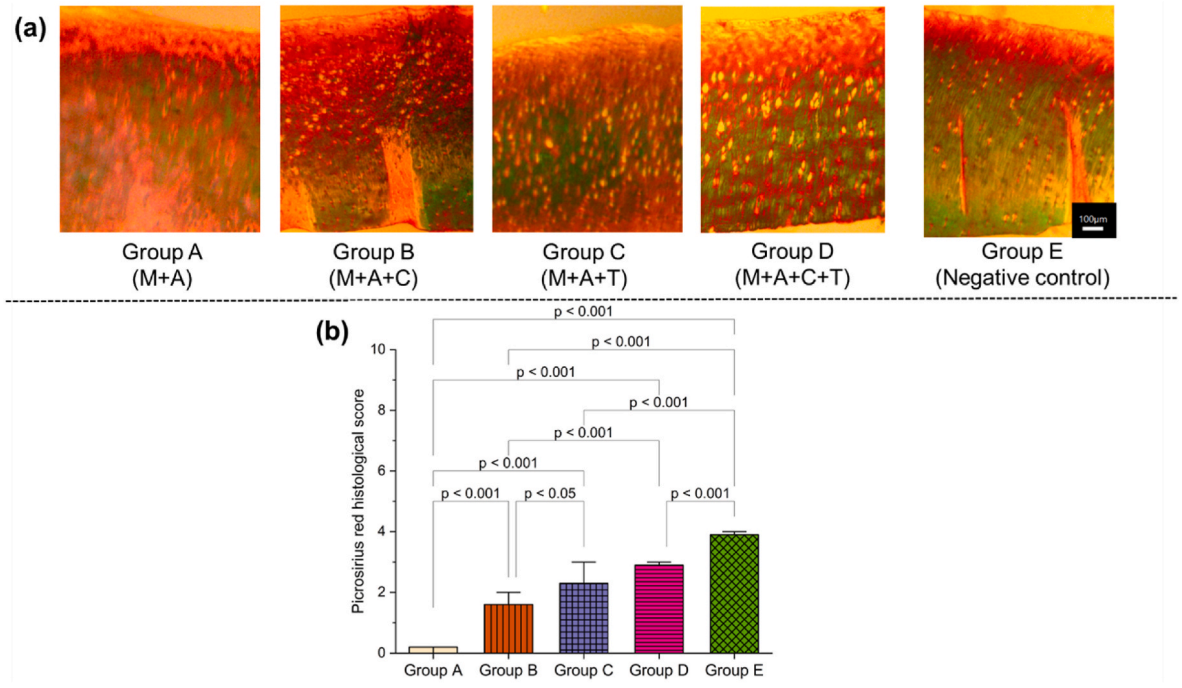

Fig. 6. Histological assessment of each treated group (n = 4 per group) of cartilage tissue, with analysis proceeding according to SZ, MZ and DZ. Note: while partially folded sections shows intensive staining, these regions were excluded from the assessment to maintain analytical accuracy (Alibegović et al., 2020) (a) Representative Picrosirius red-stained micrographs obtained via 90° rotated filter of PLM, showing variations in green colors indicative of collagen content in DZ and long and high density of collagen content in SZ by bright yellowish orange color (Coelho et al., 2018). Scale bar = 100 μm. (b) Quantitative scoring of collagen content based on the intensity of green and bright yellowish orange colors in DZ and SZ was classified as: as minimal (0), very weak (1), weak (2), moderate (3) and strong (4). The error bar shows the standard deviation of the grading. The statistical significances are shown as $p < 0.001$, $p < 0.01$, and $p < 0.05$ unless *p-values* are non-significant. Group A (M + A): samples treated with MMP-9, MMP-13 and ADAMTS-5, Group B (M + A + C): samples treated with MMP-9, MMP-13, ADAMTS-5 and COMP, Group C (M + A + T): samples treated with MMP-9, MMP-13, ADAMTS-5 and TIMP-3, Group D (M + A + C + T): samples treated with MMP-9, MMP-13, ADAMTS-5, COMP and TIMP-3, Group E (Negative control) denotes healthy samples.

DZ. Quantitative scoring of Picrosirius red staining (Fig. 6b) depicts that observers consistently assigned the lowest scores to Group A and highest to Group E, with all between-group comparisons showing statistical significance except for the comparison between Groups C and D.

3.2.3. Statistical comparison

The reliability of these histological assessments was validated through Fleiss-type weighted kappa analysis, yielding the histological scores of 0.61 and 0.53 for Safranin O and Picrosirius red staining, respectively (Alibegović et al., 2020). Positive Pearson correlation coefficients exceeding 0.50 between mechanical properties and histological findings suggests that the mechanical properties are enhanced as the histological score ascends.

3.3. Comparative biomechanics among treated groups

Fig. 7 demonstrates improvement in mechanical properties following the application of specific endogenous protease inhibitors. Group D exhibited the most pronounced and consistent improvements across all testing modalities. Young's modulus, presented in Fig. 7a, shows a substantial improvement in treated groups. Group B (M + A + C) showed more than 40 % higher Young's modulus compared to Group A,

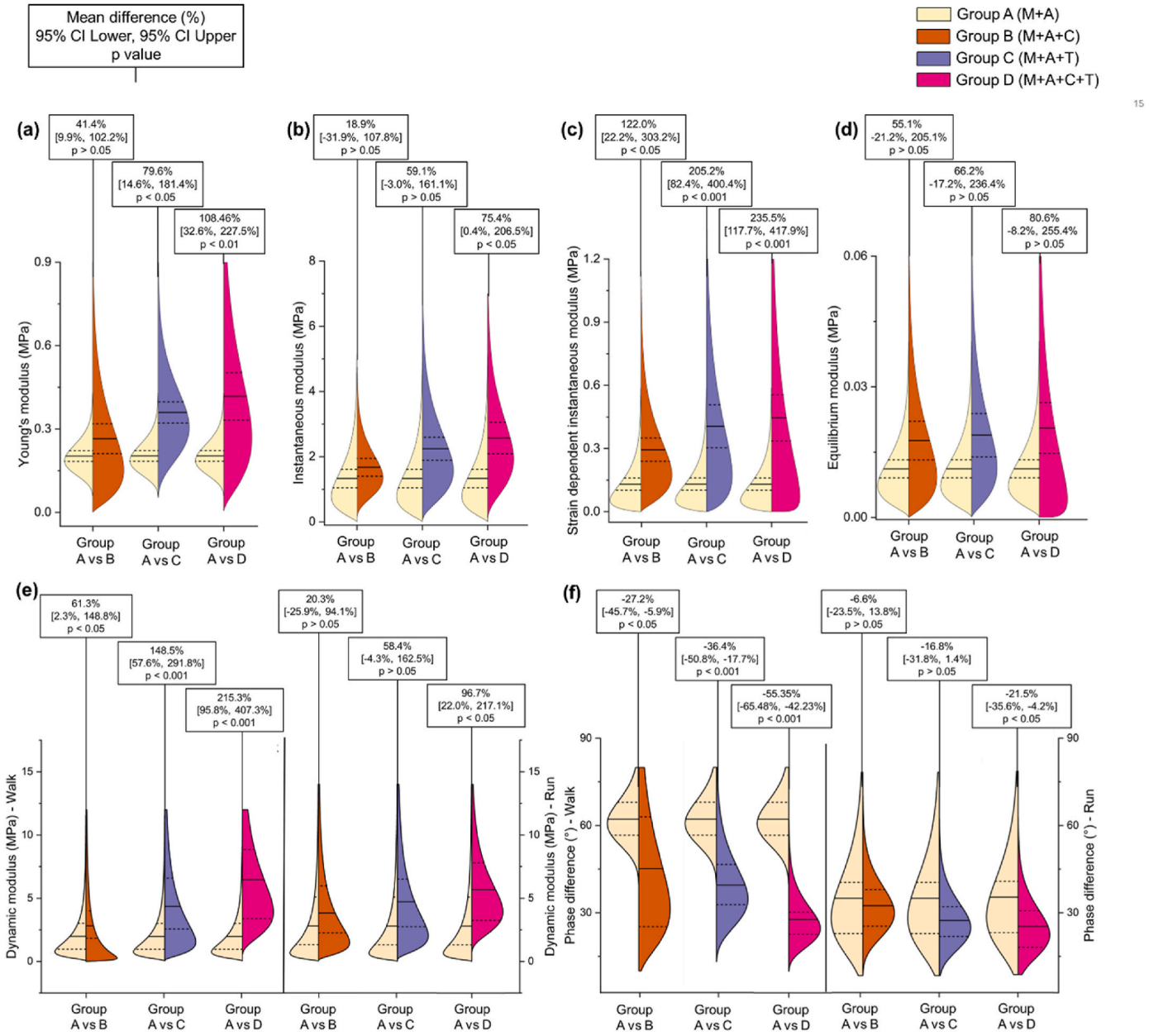

Fig. 7. Half-violin plot showing the relative improvements in mechanical properties for treated Groups B, C, and D compared to reference Group A. The percentage variations using GLM model in the boxes [mean difference% (95% CI : [*lower*, *upper*], *p* –*values*)] are calculated relative to Group A baseline values. Plots illustrate the distribution of improvements across measured parameters, with first and third quartiles (dotted line) and mean (solid line) indicated within each half-violin distribution for comprehensive assessment of treatment effectiveness. (a) Relative improvement in Young's modulus (b) Enhancement of instantaneous modulus (c) Changes in strain-dependent instantaneous modulus (d) Comparative equilibrium modulus improvements (e) Dynamic modulus enhancement patterns (f) Phase difference variations. Group A (M + A): samples treated with MMP-9, MMP-13 and ADAMTS-5, Group B (M + A + C): samples treated with MMP-9, MMP-13, ADAMTS-5 and COMP, Group C (M + A + T): samples treated with MMP-9, MMP-13, ADAMTS-5 and TIMP-3, Group D (M + A + C + T): samples treated with MMP-9, MMP-13, ADAMTS-5, COMP and TIMP-3, Group E (Negative control) denotes healthy samples.

and the addition of TIMP-3 (Group C) demonstrated nearly two-fold improvement than Group B. The instantaneous modulus analysis (Fig. 7b) depicts differential responses between the treatment groups, with mean improvements of 18.9% ($p > 0.05$, 95% CI : [−31.9%, 107.8%]) for Group B vs Group A, 59.1% ($p > 0.05$, 95% CI : [−3.0%, 161.1%]) for Group C vs Group A and a more substantial 75.4% ($p < 0.05$, 95% CI : [0.4%, 206.5%]) improvement when comparing Group D to Group A. Stress-relaxation properties (Fig. 7c and d) showed the most significant improvements among all physiological load cases. Dynamic response (Fig. 7e and f) revealed enhanced dynamic modulus and reduced phase difference during walking, indicating improved viscoelasticity. Overall, these results highlight the effectiveness of the therapeutic intervention, especially in restoring stress-relaxation and dynamic mechanical properties.

3.4. Comparison of biomechanical properties between positive and negative controls

Since Group D demonstrated significant improvement compared to degraded conditions, Fig. 8 highlights the comparison between negative control (Group E) and positive control (Group D). Fig. 8a shows the highest mean difference of 52.3 % in Young's modulus. 49.9 % of mean difference was also observed between Groups D and E. Fig. 8b exhibits the parametric change during stress relaxation between positive control and healthy cartilage by 15.4 % and 30.9 % in strain dependent instantaneous modulus and equilibrium modulus, respectively. Fig. 8c shows higher difference of dynamic (28.2 %) and phase difference (43.9 %) during walking simulation, but lower difference, 20.8 % and 25.0 % change between Group D and E during running activity.

4. Discussion

The *in vitro* OA model in this study clearly demonstrates how the combined effect of MMPs-13 and -9 and ADAMTS-5 significantly disrupted ECM macromolecules, consequently compromising the mechanical integrity of cartilage tissue across different physiological activities tested herein. The remarkable destructive potential of MMP-13 stems from its unique ability to cleave the triple-helical structure of collagen II at a rate significantly faster than other collagenases (Jean-Gilles et al., 2013). The loss of high-density collagen in SZ and DZ of Group A was observed (Fig. 6a), demonstrating an extended cleaving activity of MMP-13 throughout cartilage. Beyond targeting type II collagen, MMP-13 also degrades other ECM components including aggrercans, contributing to the comprehensive tissue degradation

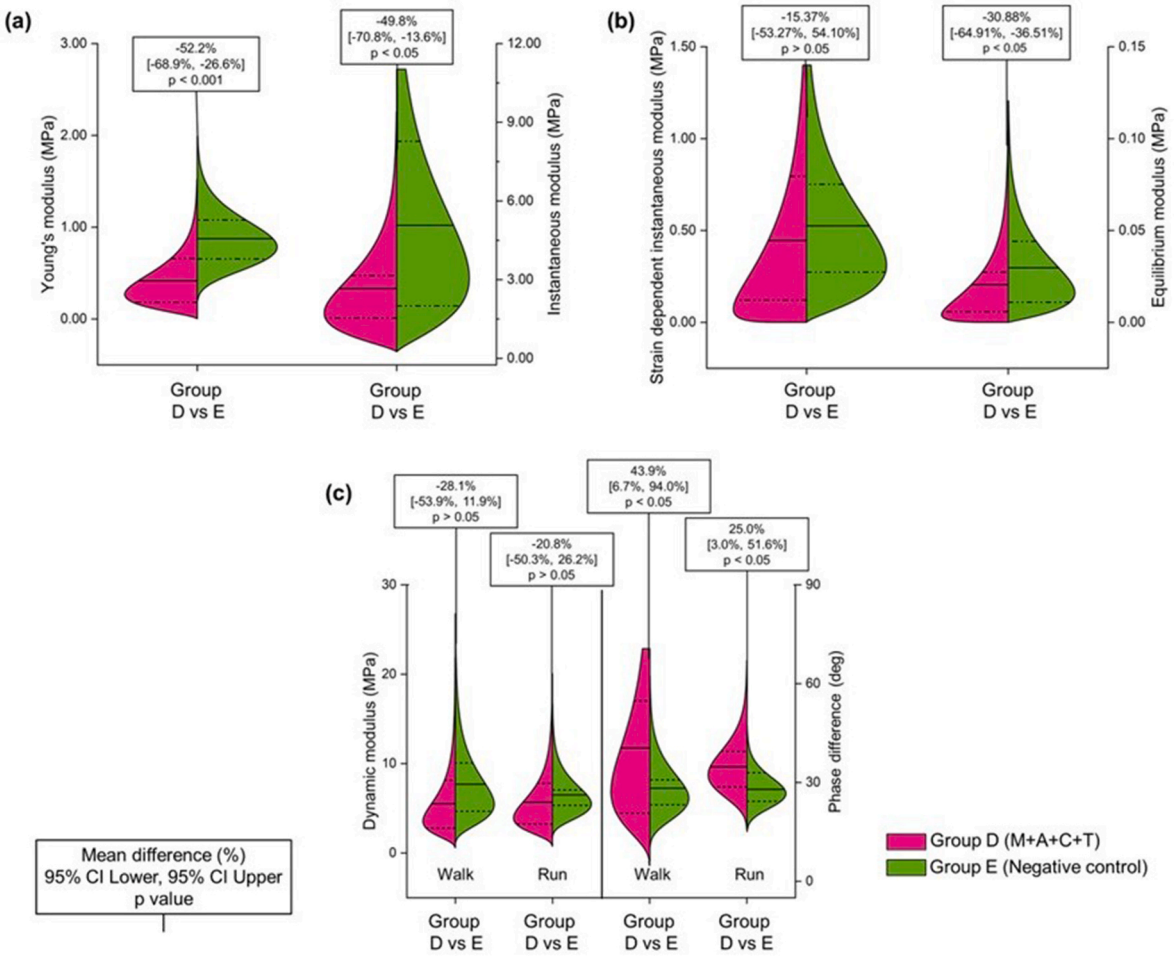

Fig. 8. Half-violin plots show the relative improvements in mechanical properties for positive Group D (M + A + C + T) compared to reference Group E (negative control). The percentage variations using GLM model in the boxes [mean difference% (95% CI : [*lower*, *upper*], $p-values$)] are calculated relative to Group E baseline values. Plots illustrate the distribution of improvements across measured parameters with reference to healthy control (Group E), with first and third quartiles (dotted line) and mean (solid line) mean indicated within each half-violin distribution. (a) Relative comparison in Young's and instantaneous modulus (b) Difference between strain-dependent instantaneous modulus and equilibrium modulus improvements of two groups (c) Dynamic modulus and Phase difference variations. Group A (M + A): samples treated with MMP-9, MMP-13 and ADAMTS-5, Group B (M + A + C): samples treated with MMP-9, MMP-13, ADAMTS-5 and COMP, Group C (M + A + T): samples treated with MMP-9, MMP-13, ADAMTS-5 and TIMP-3, Group D (M + A + C + T): samples treated with MMP-9, MMP-13, ADAMTS-5, COMP and TIMP-3, Group E (Negative control) denotes healthy samples.

(Acharya et al., 2014a; Vincenti and Brinckerhoff, 2002; Zhang et al., 2009). However, the degradation of collagen and aggrecan is a coordinated process in which MMP-13 works synergistically with other MMPs, such as MMP-9 (Hu and Ecker, 2021). Cleaved by collagenases, the fragmented collagens undergo denaturation and further degradation that results in gelatin. MMP-9 (gelatinase B) further breaks down the gelatin (compromised collagen) as well as PGs that significantly compromise cartilage's mechanical integrity (Mixon et al., 2021). Furthermore, ADAMTS-5, acting as a potent aggrecanase, accelerates PGs loss, particularly in advanced OA (Apte, 2016). The synergistic activity of these enzymes also resulted in substantial PG loss, as evidenced by the reduced Safranin O staining intensity in Group A (Fig. 5a).

The combined activity of applied proteolytic enzymes led to significant collagen and PG loss, substantially diminishing Young's modulus in Group A (Fig. 2a). Previous studies showed how collagen loss and swelling in osteoarthritis compromised instantaneous properties of cartilage (Bank et al., 2000; Bautista et al., 2016). Similarly, the extensive collagen cleavage in Group A as observed via staining intensity (Fig. 6a) in SZ explains why the compromised resistance of collagen in SZ accounts for the 71.4 % drop in instantaneous modulus relative to the negative control. PGs contribute significantly to cartilage's mechanical behavior by regulating fluid flow and controlling permeability, thereby limiting instantaneous deformation (Desrochers et al., 2012; Lu et al., 2009). During stress-relaxation, the strain dependent instantaneous modulus (at a slow strain rate) decreased by approximately 74.7 % between Groups A and E. The equilibrium modulus of Group A decreased nearly 2.6-fold compared to the negative control (Fig. 3b), primarily due to PG loss; however, collagen network degradation also contributes to this property (Julkunen et al., 2007; Korhonen et al., 2003). Moreover, reduced collagen content fails to properly constrain PGs, diminishing tissue viscosity and fluid exudation, thereby reducing elastic capacity during dynamic loading (Fig. 4a) as well as equilibrium modulus (Fig. 3b) (Linus et al., 2024; Mäkelä et al., 2014). The notably higher phase difference during dynamic activities in Group A (Fig. 4b) further confirms this relationship. Interestingly, we observed higher phase differences during walking compared to running, indicating compromised tissue viscosity due to increased permeability and fluid flow (Desrochers et al., 2012).

Our findings regarding the role of COMP provide particularly novel insights from morpho-biomechanical perspective. ECM breakdown, mechanical loading and inflammation can elevate COMP levels as the body attempts to repair defects (Cui and Zhang, 2022). Previous protein assays proved that COMP can bind to MMP-13 (Acharya et al., 2014a), MMP-9 (Ganu et al., 1998) and ADAMTS-5 (Zhen et al., 2008), preventing them from accessing their substrates and thus modulating their activity. COMP's pentameric structure bind type to collagen type I, II, and IX and hold structural integrity of ECM (Recklies et al., 1998). Cartilage degradation leads to the breakdown and release of COMP fragments (Cui and Zhang, 2022) into the synovial fluid (and blood as well) of OA patients with a significantly elevated amount (median of 3903.5 ng/mL), compared to lower levels observed in healthy individuals (Arellano et al., 2017; Keter et al., 2025; Udomsinprasert et al., 2024). Therefore, a comparatively high dose of 5000 ng/mL intact COMP was applied as a therapeutic intervention herein. This study shows significant improvement in biomechanical and macromolecular morphology of cartilages after applying COMP in Group B and Group D, which evidently substantiates that it inhibited their proteolytic activity. Based on the previous study on protein assay (Acharya et al., 2014a; Ganu et al., 1998; Zhen et al., 2008) and our histo-mechanical results, we propose that COMP can act as an active modulator of MMPs-13, -9 and ADAMTS-5 and help maintain ECM integrity by providing a competing substrate to the proteases. Moreover, COMP enables cross-bridging with several other ECM components, e.g. collagen IX, matrilins, integrins, fibronectin, and aggrecan (Acharya et al., 2014b; Cui and Zhang, 2022; Halász et al., 2007; Posey et al., 2018) that may enhance network cohesion, ameliorate mechanical response and hinder protease access from cocktail of protease using residual reacting site (Tan et al., 2009). Thus, we hypothesized that COMP indirectly inhibits the degradation of ECM's macromolecules by being a competing substrate to the overexpressed proteases. Physiologically, COMP, stimulated by mechanical loading, can circulate back into the synovial fluid, contributing to the reorganization of collagen structures (Koelling et al., 2006). This suggests that elevated COMP levels in OA could serve as a potential therapeutic strategy (Cui and Zhang, 2022)—this hypothesis is supported by the morphological findings in Group B, which showed similar PG content to Group A (Fig. 5a) but increased collagen in DZ and higher density collagen in SZ (Fig. 6a). This improvement in collagen structure translated to significant mechanical enhancements in Group B, with 41.4 %, 18.9 %, 122.0 % and 55.2 % increases in Young's, instantaneous, strain dependent instantaneous and equilibrium moduli (Fig. 7) relative to Group A. Higher collagen density also enhanced viscoelastic properties, which were evidently reflected via increased dynamic modulus (Fig. 7e) and reduced phase difference during dynamic testing (Fig. 7f).

As anticipated, treating with TIMP-3 only (Group C) significantly improved mechanical and macromolecular morphology of the cartilage tissue, as it is a stablished inhibitor of MMP-13 and ADAMTS-5 (Carreca et al., 2020; Kashiwagi et al., 2001). While TIMP-3 can bind to MMP-13 and counteract its activity, the overwhelmingly higher expression of MMP-13 compared to TIMP-3 in OA joints limits TIMP-3's capacity to regulate MMP mediated proteolysis (Carreca et al., 2020; Hu and Ecker, 2021a). Consequently, we applied an elevated amount of TIMP-3 to neutralize the activity of both collagenase and aggrecanse (Carreca et al., 2020). Although the applied amount of concentration of TIMP-3 was targeted for full inhibition of the collagenase and aggrecanase activity, Group C exhibited compromised collagen and PG content that concludes TIMP-3's inability of complete inhibition in the cocktail of proteases. Though it showed improved PG content in all zones compared to Groups A and B (Fig. 4), the histological score of Group C lies in grade 3 (weak stain). Similarly, the increased amount of collagen was observed compared to Groups A and B, but the image of Picrosirius red showed discontinuous collagen distribution in DZ (Fig. 5). Competitive binding affinity (Troeberg et al., 2012), enzyme specific kinetics (Carreca et al., 2020) and steric hindrance (Troeberg et al., 2009) in the in the mixture of protease could potentially decrease its inhibition ability significantly. The biomechanical results show that treating with only TIMP-3 (Group C) improved tissue mechanical behavior under all physiological loading conditions compared to Groups A and B (Fig. 7) by inhibiting protease activity. However, Group C's compromised morphological and mechanical properties compared to negative control (Group E) highlight a research gap needing better treatment strategies.

The addition of TIMP-3 along with COMP in Group D proved more efficacy in regulating enzymatic activities through its binding mechanism (Brew and Nagase, 2010; Carreca et al., 2020). The macromolecular morphology (Figs. 5 and 6) confirmed increased collagen across all zones and higher PG content compared to Groups A, B and C, thereby improving biomechanical properties. The increased collagen density in SZ enhanced the instantaneous modulus by 75.5 % relative to Group A. Interestingly, strain-dependent instantaneous modulus and equilibrium modulus showed remarkable improvements of by 235.5 % (Figs. 7c) and 80.6 % (Fig. 7d) compared to Group A, while Young's modulus improved by 108.5 %, despite applying the same total strain of 20 % in both tests (Fig. 7a). The properties of stress-relaxation were found improved more than Young's modulus though total strain and strain rate were same. This better performance might originate from small strain in every step along with a substantial relaxation period that let collagen networks and PGs show improved mechanical behavior. The dynamic modulus exhibited significant enhancement with a 215.4 % increase compared to Group A during walking (Fig. 4a), while 96.8 % improvement was observed during running (Fig. 4b). The reduction in phase difference followed a similar pattern, indicating improved viscoelastic response during low-frequency loading. The diminished improvement in

high-frequency response likely stemmed from insufficient collagen distribution throughout all zones and compromised PG content, which are crucial for instantaneous loading response. The higher Pearson correlation demonstrates a stronger morpho-mechanical correlation during walking, highlighting greater recovery compared to running.

Several limitations of this study warrant consideration. First, an identical Poisson's ratios across different conditions and groups were assumed. However, since the mechanical properties are considered as the bulk tissue properties, ignoring the macromolecular heterogeneity and zonal variations, this simplification may not be substantial. Second, the large standard deviations in instantaneous and stress-relaxation tests resulted in some statistically insignificant differences between groups and can be minimized by considering more samples per group. Another limitation involves the potential overestimation of instantaneous moduli by the Hayes model; however, the cartilage thickness to indenter diameter ratio in our study was less than 1, mitigating this concern (Delaine-Smith et al., 2016; Korhonen et al., 2002). Using peak values for instantaneous modulus calculation may avoid non-linearity and viscosity consideration, although rapid mechanical loading is generally considered incompressible. We evaluated the changes in macromolecular morphology using conventional semi-quantitative histological evaluation, while biochemical quantification could add important insight. Based on our biomechanical findings, we propose that the observed enhancement in mechanical performance indicates effective inhibition of protease activity by applying COMP and TIMP-3. While prior research evaluated both COMP and TIMP-3 inhibitors' efficacy against individual proteases (Acharya et al., 2014a; Carreca et al., 2020; Ganu et al., 1998; Troeberg et al., 2009; Zhen et al., 2008), this study exhibited the inhibitors efficacy against the protease mixture without evaluating the inhibitory performance against individual protease, which could provide deeper insights into its inhibitory capacity and specificity. Finally, while the inhibitory performance of COMP and TIMP-3 together is encouraging and novel, effect of elevated COMP on chondrocyte, if there is any, has not been tested in this study. COMP can affect chondrocyte behavior; either promoting collagen II synthesis (Geng et al., 2012; Li et al., 2020) or enhancing tissue invasiveness (Englund et al., 2016; Tseng et al., 2009). Since cell activity could be modulated upon different applied treatment, follow-up biological assays on live tissue in future could provide more important insights.

In conclusion, this study demonstrates COMP's modulating potential in addition to its well-established role as an OA biomarker and highlights effectiveness of TIMP-3 in enhancing morpho-mechanical properties. While exercise generally promotes joint health, identifying suitable activities of OA patients under therapeutic conditions is crucial (Petrigna et al., 2022). Our findings discourage high-impact activities like hopping or jumping for patients with enzyme-mediated OA or those treated with COMP alone, though TIMP-3 may enhance tolerance. Based on stress-relaxation results, we recommend alternating load distribution during standing and avoiding prolonged weight-bearing. Most importantly, walking appears more beneficial than running for improving cartilage health and viscous response in treated patients. This comprehensive investigation of cartilage degradation mechanisms and potential therapeutic interventions provides valuable insights into OA management. By elucidating the relationships between enzymatic activity, mechanical properties, and effective treatments, we have established a foundation for developing more targeted therapeutic and rehabilitation strategies considering both the biochemical and biomechanical aspects of cartilage function.

CRediT authorship contribution statement

Asif Istiak: Writing – review & editing, Writing – original draft, Visualization, Validation, Methodology, Investigation, Formal analysis, Data curation. **Austin Lawrence:** Writing – original draft, Investigation, Data curation. **Joseph Boesel:** Writing – original draft, Investigation, Data curation. **Md Imrul Kayes:** Investigation, Formal analysis, Data curation. **Ahmed Suparno Bahar Moni:** Writing – review & editing, Supervision, Resources, Project administration, Methodology, Conceptualization. **Tanvir R. Faisal:** Writing – review & editing, Supervision, Software, Resources, Project administration, Methodology, Conceptualization.

Role of the funding sources

Not Applicable.

Declaration of competing interest

The authors declare that they have no known competing financial interests or personal relationships that could have appeared to influence the work reported in this paper.

Acknowledgements

We acknowledge the assistance of Aaron M. McLaughlin and Melany G Musso from the New Iberia research center to use their facilities to conduct partial histological assessments.

Data availability

No data was used for the research described in the article.

References

Abbaszade, I., Liu, R.-Q., Yang, F., Rosenfeld, S.A., Ross, O.H., Link, J.R., Ellis, D.M., Tortorella, M.D., Pratta, M.A., Hollis, J.M., 1999. Cloning and characterization of ADAMTS11, an aggrecanase from the ADAMTS family. J. Biol. Chem. 274, 23443–23450.

Acharya, C., Yik, J.H., Kishore, A., Van Dinh, V., Di Cesare, P.E., Haudenschild, D.R., 2014a. Cartilage oligomeric matrix protein and its binding partners in the cartilage extracellular matrix: interaction, regulation and role in chondrogenesis. Matrix Biol. 37, 102–111.

Acharya, C., Yik, J.H.N., Kishore, A., Van Dinh, V., Di Cesare, P.E., Haudenschild, D.R., 2014b. Cartilage oligomeric matrix protein and its binding partners in the cartilage extracellular matrix: interaction, regulation and role in chondrogenesis. Matrix Biol. 37, 102–111.

Alibegović, A., Blagus, R., Martinez, I.Z., 2020. Safranin O without fast green is the best staining method for testing the degradation of macromolecules in a cartilage extracellular matrix for the determination of the postmortem interval. Forensic science. Med.Pathol. 16, 252–258.

Apte, S.S., 2016. Anti-ADAMTS5 monoclonal antibodies: implications for aggrecanase inhibition in osteoarthritis. Biochem. J. 473, e1–e4.

Arellano, R.D., Aguilar, L.S., Argüello, R., Hernadez, F., Gonzalez, F.F., Moran, J., 2017. Cartilage oligomeric matrix protein levels in synovial fluid in patients with primary knee osteoarthritis and healthy controls: a preliminary comparative analysis with serum cartilage oligomeric matrix protein. Archiv. Rheumatology 32, 189.

Atkinson, S.J., Patterson, M.L., Butler, M.J., Murphy, G., 2001. Membrane type 1 matrix metalloproteinase and gelatinase A synergistically degrade type 1 collagen in a cell model. FEBS Lett. 491, 222–226.

Bank, R.A., Soudry, M., Maroudas, A., Mizrahi, J., TeKoppele, J.M., 2000. The increased swelling and instantaneous deformation of osteoarthritic cartilage is highly correlated with collagen degradation. Arthritis Rheum.: Official J. American College Rheumatology 43, 2202–2210.

Bautista, C.A., Park, H.J., Mazur, C.M., Aaron, R.K., Bilgen, B., 2016. Effects of chondroitinase ABC-mediated proteoglycan digestion on decellularization and recellularization of articular cartilage. PLoS One 11, e0158976.

Bieth, J.G., 1995. [5] theoretical and practical aspects of proteinase inhibition kinetics. Methods in Enzymology. Elsevier, pp. 59–84.

Brew, K., Nagase, H., 2010. The tissue inhibitors of metalloproteinases (TIMPs): an ancient family with structural and functional diversity. Biochimica et biophysica acta (BBA)-molecular cell research 1803, 55–71.

Carreca, A.P., Pravatà, V.M., Markham, M., Bonelli, S., Murphy, G., Nagase, H., Troeberg, L., Scilabra, S.D., 2020. TIMP-3 facilitates binding of target metalloproteinases to the endocytic receptor LRP-1 and promotes scavenging of MMP-1. Sci. Rep. 10, 12067.

Coelho, P.G.B., Souza, M.V.d., Conceição, L.G., Viloria, M.I.V., Bedoya, S.A.O., 2018. Evaluation of dermal collagen stained with picrosirius red and examined under polarized light microscopy. Anais brasileiros de dermatologia 93, 415–418.

Collier, I.E., Legant, W., Marmer, B., Lubman, O., Saffarian, S., Wakatsuki, T., Elson, E., Goldberg, G.I., 2011. Diffusion of MMPs on the surface of collagen fibrils: the mobile cell surface–collagen substratum interface. PLoS One 6, e24029.

Cristoforetti, A., Masè, M., Ravelli, F., 2023. Model-based approach for the semi-automatic analysis of collagen birefringence in polarized light microscopy. Appl. Sci. 13, 2916.
Cui, J., Zhang, J., 2022. Cartilage oligomeric matrix protein, diseases, and therapeutic opportunities. Int. J. Mol. Sci. 23, 9253.
Davidson, R.K., Waters, J.G., Kevorkian, L., Darrah, C., Cooper, A., Donell, S.T., Clark, I. M., 2006. Expression profiling of metalloproteinases and their inhibitors in synovium and cartilage. Arthritis Res. Ther. 8, 1–10.
Delaine-Smith, R., Burney, S., Balkwill, F., Knight, M., 2016. Experimental validation of a flat punch indentation methodology calibrated against unconfined compression tests for determination of soft tissue biomechanics. J. Mech. Behav. Biomed. Mater. 60, 401–415.
Desrochers, J., Amrein, M., Matyas, J., 2012. Viscoelasticity of the articular cartilage surface in early osteoarthritis. Osteoarthr. Cartil. 20, 413–421.
Ebrahimi, M., Ojanen, S., Mohammadi, A., Finnilä, M.A., Joukainen, A., Kröger, H., Saarakkala, S., Korhonen, R.K., Tanska, P., 2019. Elastic, viscoelastic and fibril-reinforced poroelastic material properties of healthy and osteoarthritic human tibial cartilage. Ann. Biomed. Eng. 47, 953–966.
Englund, E., Bartoschek, M., Reitsma, B., Jacobsson, L., Escudero-Esparza, A., Orimo, A., Leandersson, K., Hagerling, C., Aspberg, A., Storm, P., 2016. Cartilage oligomeric matrix protein contributes to the development and metastasis of breast cancer. Oncogene 35, 5585–5596.
Festing, M., 2020. The" completely randomised" and the" randomised block" are the only experimental designs suitable for widespread use in pre-clinical research. Sci Rep. 2020 10 (1), 17577. https://doi.org/10.1038/s41598-020-74538-3PMID:33067494. Epub 2020/10/18.
Fosang, A.J., Neame, P., Hardingham, T., Murphy, G., Hamilton, J., 1991. Cleavage of cartilage proteoglycan between G1 and G2 domains by stromelysins. J. Biol. Chem. 266, 15579–15582.
Fosang, A.J., Neame, P.J., Last, K., Hardingham, T.E., Murphy, G., Hamilton, J.A., 1992. The interglobular domain of cartilage aggrecan is cleaved by PUMP, gelatinases, and cathepsin B. J. Biol. Chem. 267, 19470–19474.
Fosang, A.J., Last, K., Knäuper, V., Neame, P., Murphy, G., Hardingham, T., Tschesche, H., Hamilton, J., 1993. Fibroblast and neutrophil collagenases cleave at two sites in the cartilage aggrecan interglobular domain. Biochem. J. 295, 273–276.
Galloway, W., Murphy, G., Sandy, J., Gavrilovic, J., Cawston, T., Reynolds, J., 1983. Purification and characterization of a rabbit bone metalloproteinase that degrades proteoglycan and other connective-tissue components. Biochem. J. 209, 741–752.
Ganu, V., Goldberg, R., Peppard, J., Rediske, J., Melton, R., Hu, S.I., Wang, W., Duvander, C., Heinegård, D., 1998. Inhibition of interleukin-1α-induced cartilage oligomeric matrix protein degradation in bovine articular cartilage by matrix metalloproteinase inhibitors: potential role for matrix metalloproteinases in the generation of cartilage oligomeric matrix protein fragments in arthritic synovial fluid. Arthritis Rheum. 41, 2143–2151.
Geng, H., Nandakumar, K.S., Pramhed, A., Aspberg, A., Mattsson, R., Holmdahl, R., 2012. Cartilage oligomeric matrix protein specific antibodies are pathogenic. Arthritis Res. Ther. 14, 1–14.
Glasson, S.S., Askew, R., Sheppard, B., Carito, B.A., Blanchet, T., Ma, H.L., Flannery, C.R., Kanki, K., Wang, E., Peluso, D., 2004. Characterization of and osteoarthritis susceptibility in ADAMTS-4–knockout mice. Arthritis Rheum.: Official J. American College Rheumatology 50, 2547–2558.
Glasson, S.S., Askew, R., Sheppard, B., Carito, B., Blanchet, T., Ma, H.-L., Flannery, C.R., Peluso, D., Kanki, K., Yang, Z., 2005. Deletion of active ADAMTS5 prevents cartilage degradation in a murine model of osteoarthritis. Nature 434, 644–648.
Glasson, S., Chambers, M., Van Den Berg, W., Little, C., 2010. The OARSI histopathology initiative–recommendations for histological assessments of osteoarthritis in the mouse. Osteoarthr. Cartil. 18, S17–S23.
Grenier, S., Bhargava, M.M., Torzilli, P.A., 2014. An in vitro model for the pathological degradation of articular cartilage in osteoarthritis. J. Biomech. 47, 645–652.
Halász, K., Kassner, A., Mörgelin, M., Heinegård, D., 2007. COMP acts as a catalyst in collagen fibrillogenesis. J. Biol. Chem. 282, 31166–31173.
Hao, X., Wu, X., 2024. SP1-mediated ADAMTS5 transcription promotes IL-1β-induced chondrocyte injury via Wnt/β-catenin pathway in osteoarthritis. Mol. Med. Rep. 30, 149.
Hayes, W., Keer, L.M., Herrmann, G., Mockros, L., 1972. A mathematical analysis for indentation tests of articular cartilage. J. Biomech. 5, 541–551.
Heard, B.J., Martin, L., Rattner, J.B., Frank, C.B., Hart, D.A., Krawetz, R., 2012. Matrix metalloproteinase protein expression profiles cannot distinguish between normal and early osteoarthritic synovial fluid. BMC Muscoskelet. Disord. 13, 1–12.
Hu, Q., Ecker, M., 2021. Overview of MMP-13 as a promising target for the treatment of osteoarthritis. Int. J. Mol. Sci. 22.
Hu, X., Wu, Z., Zhang, Z., Yao, H., Wang, D.-A., 2024. Type II collagen scaffolds for tissue engineering. Commun. Mater. 5, 149.
Istiak, A., Islam, S., Adouni, M., Faisal, T.R., 2025. Hyperelastic constitutive modeling of healthy and enzymatically mediated degraded articular cartilage. Biomech. Model. Mechanobiol. 24, 471–487.
Jarecki, J., Małecka-Masalska, T., Kosior-Jarecka, E., Widuchowski, W., Krasowski, P., Gutbier, M., Dobrzyński, M., Blicharski, T., 2022. Concentration of selected metalloproteinases and osteocalcin in the serum and synovial fluid of obese women with advanced knee osteoarthritis. Int. J. Environ. Res. Publ. Health 19, 3530.
Jean-Gilles, D., Li, L., Vaidyanathan, V., King, R., Cho, B., Worthen, D.R., Chichester III, C.O., Seeram, N.P., 2013. Inhibitory effects of polyphenol punicalagin on type-II collagen degradation in vitro and inflammation in vivo. Chem. Biol. Interact. 205, 90–99.
Jiang, L., Lin, J., Zhao, S., Wu, J., Jin, Y., Yu, L., Wu, N., Wu, Z., Wang, Y., Lin, M., 2021. ADAMTS5 in osteoarthritis: biological functions, regulatory network, and potential targeting therapies. Front. Mol. Biosci. 8, 703110.
Julkunen, P., Kiviranta, P., Wilson, W., Jurvelin, J.S., Korhonen, R.K., 2007. Characterization of articular cartilage by combining microscopic analysis with a fibril-reinforced finite-element model. J. Biomech. 40, 1862–1870.
Kabir, W., Di Bella, C., Choong, P.F., O'Connell, C.D., 2021. Assessment of native human articular cartilage: a biomechanical protocol. Cartilage 13, 427S–437S.
Karsdal, M.A., Madsen, S.H., Christiansen, C., Henriksen, K., Fosang, A.J., Sondergaard, B.C., 2008. Cartilage degradation is fully reversible in the presence of aggrecanase but not matrix metalloproteinase activity. Arthritis Res. Ther. 10, 1–12.
Kashiwagi, M., Tortorella, M., Nagase, H., Brew, K., 2001. TIMP-3 is a potent inhibitor of aggrecanase 1 (ADAM-TS4) and aggrecanase 2 (ADAM-TS5). J. Biol. Chem. 276, 12501–12504.
Kersting, U.G., Stubendorff, J.J., Schmidt, M.C., Brüggemann, G.-P., 2005. Changes in knee cartilage volume and serum COMP concentration after running exercise. Osteoarthr. Cartil. 13, 925–934.
Keter, D., Thai-Paquette, V., Miamidian, J., Gulati, S., Toler, K., 2025. Synovial fluid dual-biomarker algorithm accurately differentiates osteoarthritis from inflammatory arthritis. J. Orthop. Res. 43, 304–310.
Kiani, C., Chen, L., Wu, Y.J., Yee, A.J., Yang, B.B., 2002. Structure and function of aggrecan. Cell Res. 12, 19–32.
Kim, E.M., Hwang, O., 2011. Role of matrix metalloproteinase-3 in neurodegeneration. J. Neurochem. 116, 22–32.
Knäuper, V., Will, H., López-Otin, C., Smith, B., Atkinson, S.J., Stanton, H., Hembry, R. M., Murphy, G., 1996. Cellular mechanisms for human procollagenase-3 (MMP-13) activation: evidence that MT1-MMP (MMP-14) and gelatinase A (MMP-2) are able to generate active enzyme. J. Biol. Chem. 271, 17124–17131.
Koelling, S., Clauditz, T.S., Kaste, M., Miosge, N., 2006. Cartilage oligomeric matrix protein is involved in human limb development and in the pathogenesis of osteoarthritis. Arthritis Res. Ther. 8, 1–10.
Korhonen, R., Laasanen, M., Töyräs, J., Rieppo, J., Hirvonen, J., Helminen, H., Jurvelin, J., 2002. Comparison of the equilibrium response of articular cartilage in unconfined compression, confined compression and indentation. J. Biomech. 35, 903–909.
Korhonen, R.K., Laasanen, M.S., Töyräs, J., Lappalainen, R., Helminen, H.J., Jurvelin, J. S., 2003. Fibril reinforced poroelastic model predicts specifically mechanical behavior of normal, proteoglycan depleted and collagen degraded articular cartilage. J. Biomech. 36, 1373–1379.
Kositsky, A., Linus, A., Stenroth, L., Nippolainen, E., Kröger, H., Töyräs, J., Mäkelä, J.T., Liukkonen, M.K., Tanska, P., Afara, I.O., 2025. Relationships between human patellar tendon and tibial cartilage viscoelastic properties in osteoarthritic knees: an exploratory investigation. J. Biomech., 112772
Li, Y., Tong, D., Liang, P., Lönnblom, E., Viljanen, J., Xu, B., Nandakumar, K.S., Holmdahl, R., 2020. Cartilage-binding antibodies initiate joint inflammation and promote chronic erosive arthritis. Arthritis Res. Ther. 22, 1–14.
Linus, A., Tanska, P., Nippolainen, E., Tiitu, V., Töyras, J., Korhonen, R.K., Afara, I.O., Mononen, M.E., 2024. Site-specific elastic and viscoelastic biomechanical properties of healthy and osteoarthritic human knee joint articular cartilage. J. Biomech. 169, 112135.
Lohmander, L., Neame, P.J., Sandy, J.D., 1993. The structure of aggrecan fragments in human synovial fluid. Evidence that aggrecanase mediates cartilage degradation in inflammatory joint disease, joint injury, and osteoarthritis. Arthritis Rheum.: Official J. American College Rheumatology 36, 1214–1222.
Lu, X., Mow, V., Guo, X., 2009. Proteoglycans and mechanical behavior of condylar cartilage. J. Dent. Res. 88, 244–248.
Maenohara, Y., Chijimatsu, R., Tachibana, N., Uehara, K., Xuan, F., Mori, D., Murahashi, Y., Nakamoto, H., Oichi, T., Chang, S.H., 2020. Lubricin contributes to homeostasis of articular cartilage by modulating differentiation of superficial zone cells. J. Bone Miner. Res. 36, 792–802.
Mäkelä, J., Rezaeian, Z., Mikkonen, S., Madden, R., Han, S.-K., Jurvelin, J., Herzog, W., Korhonen, R., 2014. Site-dependent changes in structure and function of lapine articular cartilage 4 weeks after anterior cruciate ligament transection. Osteoarthr. Cartil. 22, 869–878.
Marouane, H., Shirazi-Adl, A., Adouni, M., 2016. Alterations in knee contact forces and centers in stance phase of gait: a detailed lower extremity musculoskeletal model. J. Biomech. 49, 185–192.
Meehan, R.T., Regan, E.A., Hoffman, E.D., Wolf, M.L., Gill, M.T., Crooks, J.L., Parmar, P. J., Scheuring, R.A., Hill, J.C., Pacheco, K.A., 2021. Synovial fluid cytokines, chemokines and MMP levels in osteoarthritis patients with knee pain display a profile similar to many rheumatoid arthritis patients. J. Clin. Med. 10, 5027.
Meszaros, E., Malemud, C.J., 2012. Prospects for treating osteoarthritis: enzyme-protein interactions regulating matrix metalloproteinase activity. Ther. Adv. Chronic Dis. 3, 219–229.
Mixon, A., Savage, A., Bahar-Moni, A.S., Adouni, M., Faisal, T., 2021. An in vitro investigation to understand the synergistic role of MMPs-1 and 9 on articular cartilage biomechanical properties. Sci. Rep. 11, 14409.
Mixon, A., Bahar-Moni, A.S., Faisal, T.R., 2022. Mechanical characterization of articular cartilage degraded combinedly with MMP-1 and MMP-9. J. Mech. Behav. Biomed. Mater., 105131
Mukherjee, A., Das, B., 2024. The role of inflammatory mediators and matrix metalloproteinases (MMPs) in the progression of osteoarthritis. Biomater. Biosys., 100090
Nguyen, A.M., Levenston, M.E., 2012. Comparison of osmotic swelling influences on meniscal fibrocartilage and articular cartilage tissue mechanics in compression and shear. J. Orthop. Res. 30, 95–102.

Niehoff, A., Müller, M., Brüggemann, L., Savage, T., Zaucke, F., Eckstein, F., Müller-Lung, U., Brüggemann, G.-P., 2011. Deformational behaviour of knee cartilage and changes in serum cartilage oligomeric matrix protein (COMP) after running and drop landing. Osteoarthr. Cartil. 19, 1003–1010.
Petrigna, L., Roggio, F., Trovato, B., Zanghi, M., Guglielmino, C., Musumeci, G., 2022. How physical activity affects knee cartilage and a standard intervention procedure for an exercise program: a systematic review. Healthcare. MDPI 1821.
Plsikova Matejova, J., Spakova, T., Harvanova, D., Lacko, M., Filip, V., Sepitka, R., Mitro, I., Rosocha, J., 2021. A preliminary study of combined detection of COMP, TIMP-1, and MMP-3 in synovial fluid: potential indicators of osteoarthritis progression. Cartilage 13, 1421S–1430S.
Posey, K.L., Coustry, F., Hecht, J.T., 2018. Cartilage oligomeric matrix protein: COMPopathies and beyond. Matrix Biol. 71–72, 161–173.
Powell, B., Malaspina, D.C., Szleifer, I., Dhaher, Y., 2019. Effect of collagenase–gelatinase ratio on the mechanical properties of a collagen fibril: a combined Monte Carlo–molecular dynamics study. Biomech. Model. Mechanobiol. 18, 1809–1819.
Recklies, A.D., Baillargeon, L., White, C., 1998. Regulation of cartilage oligomeric matrix protein synthesis in human synovial cells and articular chondrocytes. Arthritis Rheum.: Official J. American College Rheumatology 41, 997–1006.
Rose, B.J., Kooyman, D.L., 2016. A tale of two joints: the role of matrix metalloproteases in cartilage biology. Dis. Markers 2016, 4895050.
Rosenblum, G., Van den Steen, P.E., Cohen, S.R., Bitler, A., Brand, D.D., Opdenakker, G., Sagi, I., 2010. Direct visualization of protease action on collagen triple helical structure. PLoS One 5, e11043.
Sandy, J., 2006. A contentious issue finds some clarity: on the independent and complementary roles of aggrecanase activity and MMP activity in human joint aggrecanolysis. Osteoarthr. Cartil. 14, 95–100.
Sandy, J.D., Flannery, C.R., Neame, P.J., Lohmander, L.S., 1992. J. Clin. Investig. 89, 1512.
Santamaria, S., 2020. ADAMTS-5: a difficult teenager turning 20. Int. J. Exp. Pathol. 101, 4–20.
Sarkar, S.K., Marmer, B., Goldberg, G., Neuman, K.C., 2012. Single-molecule tracking of collagenase on native type I collagen fibrils reveals degradation mechanism. Curr. Biol. 22, 1047–1056.
Schmitz, N., Laverty, S., Kraus, V., Aigner, T., 2010. Basic methods in histopathology of joint tissues. Osteoarthr. Cartil. 18, S113–S116.
Shiomi, T., Lemaître, V., D'Armiento, J., Okada, Y., 2010. Matrix metalloproteinases, a disintegrin and metalloproteinases, and a disintegrin and metalloproteinases with thrombospondin motifs in non-neoplastic diseases. Pathol. Int. 60, 477–496.
Smith Jr, G.N., 2006. The role of collagenolytic matrix metalloproteinases in the loss of articular cartilage in osteoarthritis. Front. Biosci. 11, 95.
Stojanovic, S.K., Stamenkovic, B.N., Cvetkovic, J.M., Zivkovic, V.G., Apostolovic, M.R.A., 2023. Matrix Metalloproteinase-9 level in synovial fluid—association with joint destruction in early rheumatoid arthritis. Medicina 59, 167.
Struglics, A., Larsson, S., Pratta, M.A., Kumar, S., Lark, M., Lohmander, L., 2006. Human osteoarthritis synovial fluid and joint cartilage contain both aggrecanase-and matrix metalloproteinase-generated aggrecan fragments. Osteoarthr. Cartil. 14, 101–113.
Strutzenberger, G., Claußen, L., Schwameder, H., 2021. Analysis of sloped gait: how many steps are needed to reach steady-state walking speed after gait initiation? Gait Posture 83, 167–173.
Takahashi, I., Onodera, K., Bae, J.-W., Mitani, H., Sasano, Y., Mitani, H., 2005. Age-related changes in the expression of gelatinase and tissue inhibitor of metalloproteinase genes in mandibular condylar, growth plate, and articular cartilage in rats. J. Mol. Histol. 36, 355–366.
Tan, K., Duquette, M., Joachimiak, A., Lawler, J., 2009. The crystal structure of the signature domain of cartilage oligomeric matrix protein: implications for collagen, glycosaminoglycan and integrin binding. FASEB J. 23, 2490.
Tortorella, M., Malfait, A., 2008. Will the real aggrecanase (s) step up: evaluating the criteria that define aggrecanase activity in osteoarthritis. Curr. Pharm. Biotechnol. 9, 16–23.
Tortorella, M., Pratta, M., Liu, R.-Q., Abbaszade, I., Ross, H., Burn, T., Arner, E., 2000. The thrombospondin motif of aggrecanase-1 (ADAMTS-4) is critical for aggrecan substrate recognition and cleavage. J. Biol. Chem. 275, 25791–25797.
Tortorella, M., Malfait, A.-M., Deccico, C., Arner, E., 2001. The role of ADAM-TS4 (aggrecanase-1) and ADAM-TS5 (aggrecanase-2) in a model of cartilage degradation. Osteoarthr. Cartil. 9, 539–552.
Troeberg, L., Fushimi, K., Scilabra, S.D., Nakamura, H., Dive, V., Thøgersen, I.B., Enghild, J.J., Nagase, H., 2009. The C-terminal domains of ADAMTS-4 and ADAMTS-5 promote association with N-TIMP-3. Matrix Biol. 28, 463–469.
Troeberg, L., Mulloy, B., Ghosh, P., Lee, M.-H., Murphy, G., Nagase, H., 2012. Pentosan polysulfate increases affinity between ADAMTS-5 and TIMP-3 through formation of an electrostatically driven trimolecular complex. Biochem. J. 443, 307–315.
Tseng, S., Reddi, A.H., Di Cesare, P.E., 2009. Cartilage oligomeric matrix protein (COMP): a biomarker of arthritis. Biomark. Insights 4. BMI. S645.
Udomsinprasert, W., Mookkhan, N., Tabtimnark, T., Aramruang, T., Ungsudechachai, T., Saengsiwaritt, W., Jittikoon, J., Honsawek, S., 2024. Cartilage oligomeric matrix protein as a potential biomarker for knee osteoarthritis. Bone Joint Res. 13, 261–271.
Veronesi, F., Fini, M., Giavaresi, G., Ongaro, A., De Mattei, M., Pellati, A., Setti, S., Tschon, M., 2015. Experimentally induced cartilage degeneration treated by pulsed electromagnetic field stimulation; an in vitro study on bovine cartilage. BMC Muscoskelet. Disord. 16, 1–9.
Vincenti, M.P., Brinckerhoff, C.E., 2002. Transcriptional regulation of collagenase (MMP-1, MMP-13) genes in arthritis: integration of complex signaling pathways for the recruitment of gene-specific transcription factors. Arthritis Res. Ther. 4, 157.
Wang, X., Manner, P.A., Horner, A., Shum, L., Tuan, R.S., Nuckolls, G.H., 2004. Regulation of MMP-13 expression by RUNX2 and FGF2 in osteoarthritic cartilage. Osteoarthr. Cartil. 12, 963–973.
Wetzel, M., Li, L., Harms, K.M., Roitbak, T., Ventura, P.B., Rosenberg, G.A., Khokha, R., Cunningham, L.A., 2008. Tissue inhibitor of metalloproteinases-3 facilitates Fas-mediated neuronal cell death following mild ischemia. Cell Death Differ. 15, 143–151.
Zhang, M., Zhou, Q., Liang, Q.-Q., Li, C.-G., Holz, J., Tang, D., Sheu, T.-J., Li, T.-F., Shi, Q., Wang, Y.-J., 2009. IGF-1 regulation of type II collagen and MMP-13 expression in rat endplate chondrocytes via distinct signaling pathways. Osteoarthr. Cartil. 17, 100–106.
Zhang, E., Yan, X., Zhang, M., Chang, X., Bai, Z., He, Y., Yuan, Z., 2013. Aggrecanases in the human synovial fluid at different stages of osteoarthritis. Clin. Rheumatol. 32, 797–803.
Zhen, E.Y., Brittain, I.J., Laska, D.A., Mitchell, P.G., Sumer, E.U., Karsdal, M.A., Duffin, K. L., 2008. Characterization of metalloprotease cleavage products of human articular cartilage. Arthritis Rheum.: Official J. American College Rheumatology 58, 2420–2431.